scientific reports

Check for updates

OPEN

Steam activated hydrochar from wine waste for the removal of pharmaceutical micropollutants from water

Lucio Zaccariello[1], Annarita Travaglino[2], Angelo Fenti[2]✉, Giovanni Falco[1], Simona Galoppo[2], Domenico Palma[1], Antonella Giarra[3], Maria Toscanesi[3], Marco Trifuoggi[3,4] & Pasquale Iovino[1]

This study explores the potential of hydrochar derived from grape stalks as a sustainable adsorbent for removing diclofenac (DCF), a widely used pharmaceutical and persistent water micropollutant that poses significant environmental risks if not effectively eliminated. Hydrothermal carbonization (HTC) was applied at three temperatures (200, 230, and 260 °C) to synthesize hydrochar. To further enhance its adsorption properties, the hydrochar was subjected to physical activation by steam. Comprehensive characterization, including SEM, TEM, BET analysis, and elemental composition, revealed significant chemical and morphological changes and the formation of a multy-layered porous structure, especially after steam activation. Adsorption experiments were performed under constant stirring at 100 rpm for about 24 h at room temperature. The influence of different hydrochar dosages (0.2–1.0 g L^{-1}) on the process was evaluated. The adsorption tests demonstrated that the hydrochar produced at 230 °C exhibited superior DCF removal efficiency, which was further enhanced post-activation, achieving a removal rate of up to 99.2% under optimized conditions. The experimental data for DCF adsorption onto the steam-activated hydrochar closely followed the Langmuir model, with a maximum capacity of 25.19 mg g^{-1}. Additionally, the pseudo-second-order model showed the best agreement with the experimental data. The steam-activated hydrochar derived from agricultural waste has great potential as an efficient and cost-effective adsorbent for removing DCF, addressing key challenges in water pollution and waste management.

Keywords Hydrothermal carbonization, Diclofenac adsorption, Steam-activated hydrochar, Grape stalk valorization, Sustainable water treatment

Population growth and global industrialization are causing significant environmental concerns, including depletion and contamination of water ecosystems. Among other contaminants, pharmaceutical products (PPs) dramatically increased their occurrence and concentration in water bodies due to anthropogenic activities and ineffective waste management practices. Their presence cause adverse effects to aquatic fauna, even in traces, resulting in changing of the trophic chain and risks for human health[1–3]. Diclofenac sodium (DCF), a non-steroidal anti-inflammatory drug, is the 8th best-selling pharmaceutical in the world and widely used to treat fever, inflammation, rheumatoid arthritis, polymyositis, dysmenorrhea, and body pain[4,5]. In modern countries, around 200–2300 µg of DCF per habitant are daily consumed[6]. As reported by aus der Beek et al.[7]DCF has been detected in surface water, groundwater, and tap drinking water in 50 countries around the world, with a harmful concentration between 0.032 and 18.74 µg L^{-1}. Its frequent detection as a micropollutant is due to its high solubility in water and polarity. After metabolism and excretion by human urines and faeces, unchanged DCF or/and its metabolites reach the wastewater treatment plants (WWTPs) through the sewage system[8,9]. Low concentrations of DCF do not cause toxic effects on living organisms; however, chronic exposure can cause serious damage to organs and tissues, growth disorders, and alteration of reproduction[10]. Based on that, DCF

[1]Department of Environmental, Biological and Pharmaceutical Sciences and Technologies, University of Campania "Luigi Vanvitelli", Via Vivaldi 43, 81100 Caserta, Italy. [2]Department of Engineering, University of Campania "Luigi Vanvitelli", Via Roma 29, 81031 Aversa (CE), Italy. [3]Department of Chemical Sciences, University of Naples Federico II, Via Vicinale Cupa Cintia 26, 80126 Naples, Italy. [4]CeSMA-Advanced Metrological and Technological Services Centre, University of Naples Federico II, Corso Nicolangelo Protopisani, 80146 Naples, Italy. ✉email: angelo.fenti@unicampania.it

has been listed on the "Watch List" by EU Decision 2015/495, which includes compounds of high environmental concern that must be removed from aquatic systems through cost-effective treatment methods[9]. Due to its low volatility, hydrophobicity, poor biodegradability, and complex structure, DCF cannot be completely removed by conventional wastewater treatment processes, resulting in its continuous accumulation in water bodies[11]. Efficiently removing DCF from wastewater is crucial since it could eliminate the dangers associated with its presence in the ecosystem[4,12].

Up to now, several technologies have been successfully applied for DCF removal, including reverse osmosis, membrane filtration, chemical precipitation, and advanced oxidation processes (AOPs), among others[13–15]. However, these processes have inherent shortcomings, notably membrane fouling, high procurement, and toxic by-product generation[16]. As an alternative approach, adsorption has proven to be a successful technique because of its simplicity, wide applicability, and no harmful by-product generation[17,18]. Adsorption materials like biochar, and coal-based materials, often used as precursors for producing activated carbons, exhibit poor chemical stability, low adsorption capacities, high cost, restricted pores, and environmental unsustainability. Consequently, they are ineffective at removing organic molecules from contaminated water[16,19].

The development of new adsorbents with lower cost and higher adsorption capacities is urgently required[20,21]. In pursuit of resource preservation and waste valorization, increased attention has recently been focused on agricultural waste biomass, which can be transformed into efficient adsorbent materials[22,23].

The winemaking sector produces around 20 million tons of by-products annually, including grape skins, seeds, and stalks. Managing this substantial waste output during the production season presents a major environmental challenge. Traditional disposal methods, such as composting and landfilling, carry significant risks, as the high moisture and nutrient content of these residues can contribute to the spread of pests and diseases. Consequently, it is essential to develop sustainable and environmentally friendly solutions that align with the unique properties of these by-products.

Various thermochemical processes are able to convert carbon-based materials into carbon-rich products. These techniques include flash carbonization, gasification, and pyrolysis[24–26]among others. While these processes offer several advantages, they also exhibit limitations that hinder their broader application in wastewater treatment practices. Flash carbonization is a high-energy demand technique, gasification produces a small amount of carbonaceous material and a tarry by-product that is difficult to handle[27,28]while pyrolysis is not suitable for high moisture biomass waste[29,30].

In this context, hydrothermal carbonization (HTC) has recently gained more attention as a technique for upgrading wet biomass into efficient and low-cost adsorbents. The HTC process offers the significant advantage of eliminating the need for biomass pre-drying, which reduces energy requirements compared to other thermochemical methods. In this process, also known as wet pyrolysis, the biomass is heated at moderate temperatures, ranging from 180 to 260 °C, in a closed chamber under autogenous pressure to produce a carbonaceous material[29,30]. During HTC, alterations occur in the polarity, dielectric constant, and ionic product of water molecules. The fluctuations in these properties are an inherent feature of hydrothermal carbonization, as they enable the formation of reaction pathways that are not achievable in other conversion methods, such as pyrolysis[31]. The process involves several types of reactions, including hydrolysis, dehydration, decarboxylation, isomerization, and condensation-polymerization, among others. These reactions lead to the formation of a porous solid material, rich in surface functional groups, known as hydrochar. The yield, particle size, porosity, and surface chemistry of hydrochar are mainly affected by factors, such as temperature, reaction time, and water-to-biomass ratio used during the HTC treatment. This resulting material is recognized for its potential uses as a fuel, a soil amendment to improve soil fertility, and a low-cost adsorbent for removing organic contaminants from water[29,32–34].

Hydrochar can exhibit low surface area and porosity, primarily due to the feedstock characteristics, low severity of operating conditions, and formation and deposition on the surface of secondary hydrochar, which hampers its adsorption effectiveness. Generally, two primary modification methods are employed to improve hydrochar physicochemical properties: chemical activation and physical activation[31]. In physical activation, steam, nitrogen, or carbon dioxide are used to mildly reduce the carbonaceous material. Conversely, chemical activation involves mixing a chemical dehydrating agent into the biomass before the activation process. Nonetheless, both methods require heat. Although chemical activation usually produces higher-quality activated carbon, physical activation is often preferred due to its lower chemical consumption, leading to reduced costs[35,36].

Most research has primarily focused on lab-scale HTC reactors, typically with reaction volumes of a few millilitres. Small-scale setups present several limitations, such as difficulty in replicating industrial conditions, potential for misleading data due to transport limitations, and challenges in accurately defining scale-up parameters. Less is reported about the operations of this process at larger reactor scale. Pilot-scale reactors offer several advantages, mainly related to the mitigation of the financial and operational risks associated with scaling up directly from small lab-scale setups. Accordingly, in this study, an HTC reactor with a reaction volume of 3 L was used to investigate the effect of reaction temperature, the most relevant operating condition, on the production of an efficient and cost-effective absorbent for removing DCF from impacted water by using grape stalks as raw material. The produced hydrochar was physically activated through the steam activation method to improve its adsorption characteristics, while much of the research has concentrated on chemical activation, which raises environmental concerns and entails high operation and maintenance costs. The physiochemical properties of pristine and activated hydrochars were well-characterized by scanning electron microscopy (SEM), transmission electron microscopy (TEM), Brunauer-Emmett-Teller (BET) method, and elemental analyses. Finally, adsorption isotherms and kinetics were evaluated to determine the feasibility of the DCF adsorption process onto hydrochar.

Apart from the novelty represented by the use of a larger-scale HTC reactor, the approach outlined in this article presents greater technical practicality and environmental sustainability by addressing key challenges in the waste management of a worldwide abundant agricultural by-product.

Materials and methods

Chemicals

Diclofenac sodium salt (CAS: 15307-79-6) was provided by Alfa Aesar (Ward Hill, Massachusetts, Acetonitrile for HPLC (99.9%) and formic acid (98.0%) were provided from Honeywell (Seelze, Germany). Sodium hydroxide (J.T.Baker) and chloridric acid (37.0%, Sigma-Aldrich, UK) were used to adjust the solution pH if necessary. All solutions were prepared with Milli-Q water (18.2 MΩ cm^{-1} resistivity, 25 °C) from an Elix ® Essential 10 UV water purification system (Merck, Darmstadt, Germany).

Feedstock preparation

The grape stalks used to synthesize the hydrochar were provided by a wine-distillery facility located in the Lazio region, Italy. The biomass underwent multiple washes with distilled water to eliminate impurities, followed by rinsing with milliQ water and overnight drying at 80 °C. Next, the dried material was crushed and sieved to obtain a particle fraction ranging from 1 to 2 mm. Finally, the resulting feedstock was stored in a tightly sealed flask for subsequent use.

The hydrothermal carbonization experimental apparatus and testing procedure

The HTC experimental setup used for the hydrochar production is composed of three main sections: a reactor, a heat exchanger, and a condenser (Fig. 1). The HTC reactor is a stirred batch reactor made of AISI 316 L stainless steel with a reaction volume of 3 L. Heating is provided by two electric heating elements with an overall power of 2.4 kW. The reaction temperature is ensured by a control loop incorporating a thermocouple (T1) connected to the reactor bottom, a comparator receiving the temperature set-point, and a voltage controller for adjusting the current flow to the resistance. The top of the reactor is equipped with a flange housing various connector: three for thermocouples (T1, T2 at the bottom, and T3 at the top), one for the shaft of the mechanical agitator, and one for gas exit. The reactor can operate at a maximum permissible temperature of 300 °C and a pressure of approximately 100 bars. Further details on the experimental setup can be found elsewhere[37].

The lab-scale HTC reactor was operated with a reaction mixture composed of 800 mL of distilled water and 80 g of grape stalks (GS), to obtain a water/biomass ratio (R) equal to 10 (Eq. 1):

$$R = \frac{W_{H_2O}}{W_{GS}} \tag{1}$$

where W_{H_2O} is the mass of the water in the reaction mixture and W_{GS} is the mass of the dried grape stalks.

The hydrochar obtained from the HTC tests underwent multiple washes with distilled water to eliminate impurities, followed by rinsing with milliQ water and overnight drying at 80 °C. Then, the dried hydrochar was sieved again to obtain particles in the range of 1–2 mm for the steam activation process.

The HTC process occurs in subcritical water under relatively mild conditions, with a reaction temperature commonly maintained in a range of about 180–260 °C and typical residence time ranging from 1 to 8 h, under autogenous pressure[29,38,39]. Temperature is the primary factor influencing the HTC process because it determines the properties of water, which in turn affect the ionic reactions that occur in the subcritical region. When the temperature exceeds the activation energy, several reactions take place, including dehydration, decarboxylation,

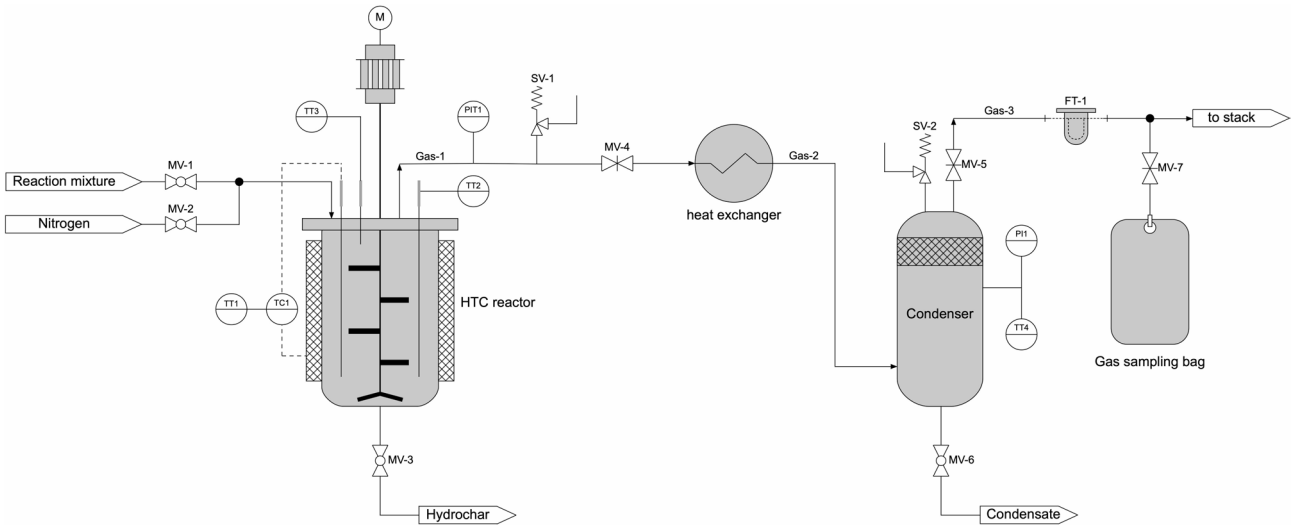

Fig. 1. Schematic illustration of the lab-scale HTC apparatus.

and condensation. Residence time also influences hydrochar characteristics, although temperature has a more pronounced effect. Therefore, to select a hydrochar with effective adsorption characteristics, the experimental tests were conducted across a wide temperature range of 200, 230, and 260 °C, with a moderate reaction time of 4 h[40–42].

The conversion efficiency of GS into hydrochar was expressed as mass yield (MY), which was calculated using Eq. 2:

$$MY = \frac{W_{HC}}{W_{GS}} \tag{2}$$

where W_{HC} and W_{GS} are the dry mass of the hydrochar and grape stalks.

The hydrochar activation apparatus and testing procedure

Figure S1 shows the experimental setup used for activating hydrochar. It can be schematically divided into three sections: an activation reactor, a heating system, and a steam generator. The activation reactor, made of AISI 310S stainless steel, has a nominal diameter of 1 ¼" and a height of 1.10 m. A perforated plate, 3 mm thick with 2 mm holes, is positioned at 70 cm from the bottom flange to support the hydrochar and uniformly distribute the activating medium (steam). The heating system consists of two semi-cylindrical ceramic fiber heaters with a total power of 3.50 kW, which is able to reach a maximum operative temperature of 1100 °C. The temperature control is achieved using a thermoregulator and a type K thermocouple located at the base of the perforated plate. The steam generator, made of AISI 304 stainless steel, is a 2 L cylinder with a 0.50 kW wire heater, producing a maximum steam flow rate of 10 g min^{-1} at a temperature of 250 °C. A precision pump with an adjustable flow rate supplies water to the steam generator unit.

Several studies on the steam activation of biomass-derived carbon materials showed that the optimal temperature and residence time for enhancing both pore diameter and surface area fall within the range 700–900 °C and 15–120 min, and that temperature has a more significant impact on these parameters than reaction time[43,44]. However, increasing both temperature and residence time results in a decrease in the mass yield of activated carbon. Therefore, to produce activated hydrochar with a substantial surface area and an acceptable production yield (higher than 50 wt%), the hydrochar activation tests were conducted at 900 °C for 15 min. Additionally, a steam flow rate of 5 g m^{-1} was selected. Preliminary tests indicated that this flow rate effectively limits the loss of activated hydrochar particles from the reactor to less than 2%.

Grape stalks and hydrochar characterization

Elemental analysis and determination of ash content were carried out on the starting grape stalks and on the pristine and steam-activated hydrochars. Moreover, characterization analyses, including determination of point zero charge (pH_{pzc}), SEM, TEM, and S_{BET} analyses were performed on the non- and steam-activated hydrochars.

Elemental analysis, ash content, and calorific value of grape stalks and hydrochars

The elemental composition of the grape stalks and hydrochars, including the mass fractions of carbon, hydrogen, nitrogen, sulphur, and oxygen (by difference) was determined using a LECO CHN-S 628 analyzer. This measurement method relies on complete and instantaneous oxidation, accomplished through pure oxygen (dynamic flash combustion) of the samples, resulting in their conversion into gaseous products. Quantitative estimation is then achieved using either non-dispersive infrared (IR) or thermal conductivity cells. The ash content was determined after drying the sample in an oven at 105 °C for 12 h and then placing it in a muffle furnace at 600 °C for 4 h. Once the muffle furnace cooled, the ash content was calculated. The percentage was determined by the weight difference relative to the initial weight.

The higher heating value (HHV) of both materials was evaluated using a correlation proposed by Channiwala and Parikh[45]:

$$HHV = 349.1C + 1178.3H + 100.5S - 103.4O - 15.1N - 21.1Ash \tag{3}$$

where *C*, *H*, *S*, *O*, *N*, and *Ash* are percentages of carbon, hydrogen, sulfur, oxygen, nitrogen, and ash reported on a dry basis.

This correlation has a wide range of applicability, from biomasses and carbonized materials to more complex wastes[46,47].

Determination of the point zero charge

The zero-charge pH (pH_{pzc}) of the hydrochar was determined through pH titration, as reported in a previous study performed by Salvestrini et al.[17]. Briefly, forty milliliters of 0.01 M NaCl solution were dispensed into 50 mL test tubes, and the pH was adjusted to a value ranging from 2 to 10 by adding a few drops of 0.1 M HCl or 0.1 M NaOH solution. Twenty milligrams of hydrochar were added to each solution, and after 48 h, the final pH was measured and plotted against the initial pH. The pH at which the curve pH_{final} vs. $pH_{initial}$ intersected the line $pH_{final} = pH_{initial}$ provided the pH_{pzc} of hydrochar.

Scanning electron microscopy (SEM) and trasmission electron microscopy (TEM)

Hydrochar samples were analyzed by SEM and TEM to analyze the morphology and surface composition of the hydrochar. For SEM analysis, samples were placed on an alumina stub covered with carbon tape and then a thin conductive layer of Au-Pd was sputtered using a sputter coater (Desk V, Denton Vacuum, USA). SEM images were collected with Nova NanoSEM 450 microscope (FEI ThermoFisher Scientific, Waltham, USA) at an

accelerating voltage of 3 kV, using an Everhart Thornley Detector (ETD) and a Through Lens Detector (TLD) for the highest magnifications.

Hydrochar samples were prepared for TEM analysis by ultrasonically suspending the powder sample in ethanol and placing 5 µL drop of the suspension on a holey carbon-coated copper grid (200 mesh) for 1 min. After removing excess solvent with filter paper, grids were air-dried and then introduced to the TEM microscope. TEM microscope FEI TECNAI G2 S-twin (FEI ThermoFisher Scientific, Waltham, USA) was operated at an acceleration potential of 120 kV equipped with a LaB_6 source.

Hydrochar specific surface area

The specific surface area (S_{BET}) of the studied materials were estimated from nitrogen adsorption-desoprtion isotherms using the Brunauer-Emmett-Teller (BET) model. For N_2 isotherms at a temperature of 77 K, the BET model was evaluated in the pressure range of P/P_o = 0.01–1.00. The analyses were performed with an automatic analyzer (Micromeritics TriStar 3030 Plus instrument). The samples were previously treated in the sample cell at 180 °C under vacuum for up to 3 h, until complete degassing was achieved[48].

Diclofenac adsorption experiments

Following each specific treatment, pristine and activated hydrochar underwent thorough washing with milliQ water and subsequently dried in an oven at 105 °C overnight to eliminate impurities. This washing process was repeated three times. Once the samples were dried, them underwent sieving using an aluminum sieve (Endecotis LTD, London, England, S.N. 326125): one portion with a particle size less between 0.5 and 1 mm, and the other with a particle size in the range of 1–2 mm. For the DCF adsorption tests, the latter hydrochar portion was used. Then the samples were placed in the oven at 80 °C for 1 h before use, in order to release any adsorbed impurities. In each adsorption test, the initial concentration of DCF (C_0) was 5.0 mg L^{-1}.

A specific amount of hydrochar was added into falcon tubes, allowing it to interact with the DCF solution (50 mL). Subsequently, the tubes were subjected to a constant agitation at 100 rpm for roughly 24 h at room temperature. The impact of different adsorbent dosages (0.2–1.0 g L^{-1}) on the process was investigated. Detailed experimental conditions for each adsorption test are provided in Table S1.

Kinetic studies and adsorption isotherms

The adsorption capacity (mg g^{-1}) of the optimized adsorbent was determined from mass balance analysis[49,50]:

$$q_e = \frac{C_0 - C_e}{X} \tag{4}$$

where C_0 and C_e are the initial concentration and the concentration at the equilibrium of DCF in the solution, respectively, and X is the adsorbent dosage, i.e. the mass of hydrochar to the liquid volume ratio (g L^{-1})[51].

The assessment of adsorption performance was carried out in terms of DCF removal (%):

$$DCF\ removal\ (\%) = \frac{DCF\ (t=0) - DCF\ (t)}{DCF\ (t=0)} \times 100 \tag{5}$$

The relationship between the concentration of the adsorbate in the adsorbent phase (q_e) and in the liquid phase (C_e) is defined as the adsorption isotherm[52]. The experimental data were fitted using Langmuir, Freundlich, Dubinin-Radushkevich (D-R), and Temkin models to determine adsorption isotherms (Eqs. (6), (7), (8) and (9))[53–55].

$$q_e = \frac{q_{max} k_L C_e}{1 + k_L C_e} \tag{6}$$

$$q_e = k_F {C_e}^{1/n} \tag{7}$$

$$ln(q_{e)} = \ln(q_{max}) - B_{D-R} * \epsilon^{\,2} \tag{8}$$

$$q_e = B \ln (K_T C_e) \tag{9}$$

where q_e is the amount of DCF adsorbed per unit mass of hydrochar at equilibrium (mg g^{-1}), q_{max} is the maximum amount of DCF adsorbed on the unit mass of hydrochar (mg g^{-1}), K_L is the Langmuir adsorption constant (L g^{-1}), K_F is the Freundlich constant, and n represents and empirical parameters that depends on the degree of heterogeneity of adsorbing sites. $B_{D\text{-}R}$ represents the Dubinin–Radushkevich constant (mol^2 kJ^{-2}), while $\varepsilon = RT\ln(1 + 1/C_e)$ denotes the Polanyi potential (kJ mol^{-1})[56]. B (J mol^{-1}) and K_T (L g^{-1}) are the Temkin isotherm constants, related to the heat of adsorption and the adsorption equilibrium, respectively.

The Langmuir isotherm theory involves the formation of a single layer of adsorbate on a uniform adsorbent surface. The model relies on three key assumptions: (i) all adsorption sites are uniform in size and shape; (ii) each site has an equal likelihood of being vacant and can accommodate only one pollutant molecule; (iii) the heat energy released during adsorption is uniform for each site. The Freundlich sorption equation is an empirical model that is particularly well-suited for isotherm data that do not reach a saturation point[57]. The D–R isotherm model is based on the assumption that adsorption occurs as a multilayer process, primarily governed by van der Waals forces. It is particularly suited for describing physical adsorption phenomena on porous and heterogeneous surfaces. The Temkin isotherm model describes adsorption using a two-parameter equation,

assuming monolayer adsorption on a heterogeneous surface. It considers the effects of adsorbent–adsorbate interactions, and proposes that the heat of adsorption decreases linearly with increasing surface coverage[58].

Furthermore, to quantify the changes in adsorption with time and to evaluate kinetic parameters, four classical kinetic models, including pseudo-first (PFO) and pseudo-second order (PSO), Intra-particle diffusion (IPD), and Elovich models were used. The PFO model is generally for physical adsorption (Eq. 10), while the PSO is for chemical adsorption (Eq. 11)[53]. The IPD model, based on the Morris and Weber approach, is employed to investigate the rate-controlling steps in adsorption, including surface interaction, pore diffusion, film resistance, and mass transfer mechanisms. The Elovich model describes chemisorption processes on heterogeneous surfaces. It assumes that the adsorption rate decreases exponentially as the surface becomes more covered, due to the increasing energy barrier for adsorption[59]:

$$q_t = q_e(1 - e^{(-k_1 t)}) \tag{10}$$

$$q_t = \left(\frac{{q_e}^2 k_2}{1 + q_e k_2}\right) t \tag{11}$$

$$q_t = k_{id} t^{1/2} \tag{12}$$

$$q_t = \alpha + \beta \ln(t) \tag{13}$$

where q_t (mg g^{-1}), q_e (mg g^{-1}), k_1 (min^{-1}), k_2 (mg g^{-1} min^{-1}) and t (min^{-1}) are the adsorption amount of DCF at any time, the adsorption amount of DCF at equilibrium, the rate constants of the PFO and PSO related models, and the adsorption time, respectively. k_{id} (mg g^{-1} $min^{-1/2}$) represents the rate constant of the intraparticle diffusion (IPD) model. Finally, α (mg g^{-1} min^{-1}) and β (g mg^{-1}) correspond to the adsorption rate during the initial phase and the desorption constant, respectively[60].

Analytical methods

At specific time intervals, samples of DCF solution were extracted from the adsorption falcon tubes and subjected to analysis, following a previous study[14]using high-performance liquid chromatography (HPLC, Shimadzu, model CBM-20 A) equipped with a UV diode array detector (DAD). A C18 column (150 mm–2.1 mm, 5 µm) served as the stationary phase. The mobile phase comprised a mixture of acetonitrile and formic acid (0.1%) in Milli-Q water, with a ratio of 60:40 (v/v), flowing at a rate of 1.0 mL min^{-1}. The analyses were conducted under isocratic conditions at room temperature, with an injection volume of 20 µL. Quantitative analysis of DCF was performed using an absorbance–concentration calibration curve at 276 nm, demonstrating linearity within the range of 0.5–20.0 mg L^{-1}. To verify the instrument's absorbance linearity, a certified standard solution of 10 mg L^{-1} caffeine (Shimadzu Corporation, Japan) was employed. The limits of detection (LOD) and quantification (LOQ) were determined to be 0.056 mg L^{-1} and 0.160 mg L^{-1}, respectively.

Results and discussions

Hydrochar preparation and characterization

HTC experiments and hydrochar activation

The lab-scale HTC reactor was operated at three reaction temperatures (200, 230, and 260 °C) and at a fixed reaction time (4 h). As aforementioned, for each HTC test, the reaction mixture was prepared to obtain a water-to-biomass ratio equal to 10.

Table 1 reports the main chemical properties and calorific value of GS. The elemental analysis shows that GS has contents of C, H, O, N, and ash consistent with typical values of common lignocellulosic biomasses. Therefore, the calorific value is also coherent.

The temperature and pressure trends recorded during the experimental runs are displayed in Fig. 2. It can be observed that the HTC apparatus took from 35 min to 60 min to reach the set-point temperature. Thus, the residence time was calculated from the instant the set-point temperature was reached for the first time to the start of the cooling down process. After an initial slight peak, due to the delay of heat transfer between the external surface of the reactor (heated by the external heater) and the temperature inside the reactor, the temperatures stabilized very close to the set-point, i.e., mean temperature ± 2 °C. A similar trend was observed for the pressure profiles inside the reactor, which stabilized at approximately 18 bars, 28 bars, and 46 bars for the tests conducted respectively at 200, 230, and 260 °C.

As far as non-activated hydrochar is concerned, its carbon content increased from 65.55 wt% to 73.67 wt% as the reaction temperature rose from 200 to 260 °C (Table 2). On the contrary, hydrogen and oxygen decreased from 5.37 wt% to 5.10 wt%, and from 25.19 wt% to 16.90 wt%, respectively. Nitrogen and ash stabilized around 1.10 wt% and 3.20 wt%. These results indicated that the HTC process, on the one hand, produced the enrichment of hydrochar in carbon; on the other hand, favored the migration of hydrogen and oxygen in the

Elemental analysis, wt% $_{d.b.}$					Inorganics, wt% $_{d.b.}$
C	H	O[a]	N	S	Ash
45.95	6.97	44.05	0.63	< 0.1	2.40

Table 1. Elemental analysis, Ash content, and calorific value of grape stalks. wt = weight basis. d.b.=dry basis. [a]Estimated by difference.

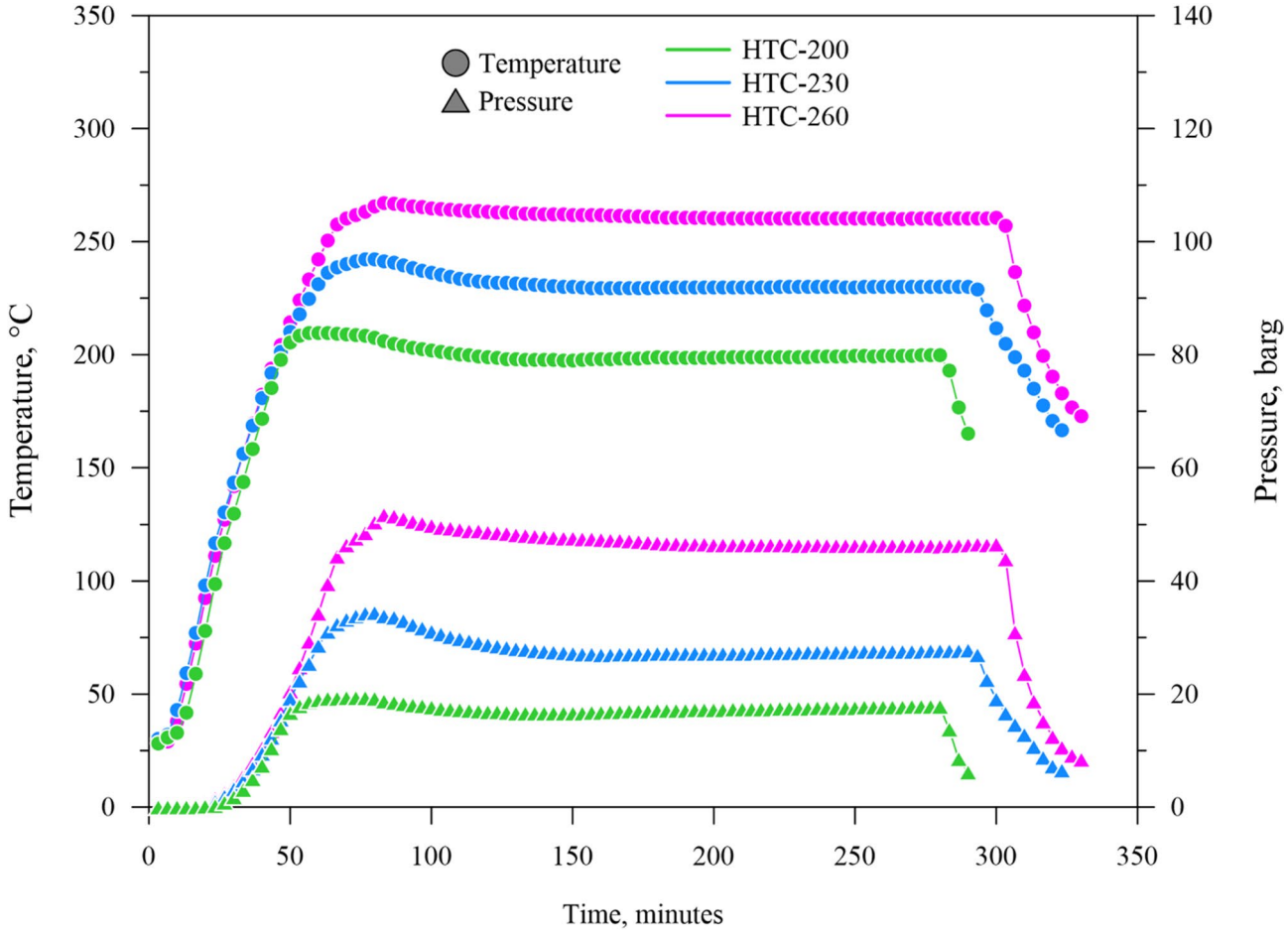

Fig. 2. Temperature and pressure trends during experimental runs performed at 200, 230, and 260 °C.

	Elemental analysis, wt% $_{d.b.}$					Inorganics, wt% $_{d.b.}$	Yield, wt./wt.
Test ID	C	H	O[a]	*N*	S	Ash	MY
HC-200	65.55	5.37	25.19	0.98	< 0.1	3.24	0.78
HC-230	66.98	5.23	23.43	1.14	< 0.1	3.22	0.67
SA-HC-230	88.06	2.12	5.06	1.72	< 0.1	5.05	0.43
HC-260	73.67	5.10	16.90	1.11	< 0.1	3.22	0.62

Table 2. Elemental analysis, Ash content, and calorific value of hydrochars. wt = weight basis. d.b.=dry basis. [a]Estimated by difference. MY = mass yield.

liquid and gaseous phases. This behavior is attributed to depolymerization, dehydration, decarboxylation, and aromatization reactions, which result in a coalification-like process[29]. This is consistent with the increase in the hydrochar HHV that progressively moved from 26.42 MJ kg^{-1} to 29.86 MJ kg^{-1} as the reaction temperature increased from 200 °C to 260 °C. On the other hand, the yield of hydrochar decreased from 0.78 to 0.62. These results can be explained by considering the key role of temperature in the HTC process. Temperature provides thermal energy for the cleavage of the biomass chemical bonds. Higher temperatures favor the migration of atoms from the solid biomass to the liquid and gaseous phases generated during the process, which necessarily leads to a decrease in the hydrochar yield. Similar results were found by Yu et al.[61].

Activated hydrochar (SA-HC-230) exhibits a significant increase in carbon (+32.28%) and an impressive reduction in oxygen (-78.40%) when compared to the non-activated hydrochar produced at the same HTC temperature (230 °C). These changes may result from the further removal of carbonyl and carboxyl groups (R1,2) as well as from the extension of the water-gas reaction (R3). Additionally, the very high temperature of the steam activation process may enhance combustion reactions involving the carbon and oxygen present in the hydrochar. The increase in carbon content of the activated hydrochar reveals the predominant role of decarbonylation and decarboxylation reactions over the water-gas reaction. This hypothesis is supported by the observed reduction in the yield of activated hydrochar.

$$RCOR' \rightarrow CO + RR' \quad \text{(R1)}$$

$$RCOOR' \rightarrow CO_2 + RR' \quad \text{(R2)}$$

where $RCOR'$ and $RCOOR'$ represent carbonyl and carboxyl sites contained in the hydrochar, respectively.

$$C_{(hydrochar)} + H_2O \leftrightarrow CO + H_2 \quad \text{(R3)}$$

Point of zero charge

The pH_{pzc} represents the pH level where the surface charge of the material neutralizes, aiding in discerning the hydrochar surface charge across various pH levels. Below the pH_{pzc} ($pH < pH_{pzc}$), hydrochar carries a positive charge, while above this value ($pH > pH_{pzc}$), the surface adopts a negative charge. DCF, with a pK_a of 4.22, acts as a weak electrolyte. In water, it predominantly exists in its neutral form at pH values below 4.22, transitioning to a more prevalent anionic form at pH values above 4.22[12]. In Fig. S2, the zero-charge pH of HC-230 (red line) and SA-HC-230 (blue line) were measured as 6.0 ± 0.1 and 7.1 ± 0.1, respectively. Under the experimental pH conditions used (9.0 ± 0.1), both pristine and SA-HC-230 surfaces exhibit a negative charge, while DCF is primarily present in its anionic form, leading to electrostatic repulsion between the contaminant and the sorbent surface. Hence, it is presumed that several other mechanisms, such as interactions between surface functional groups, hydrogen bonding, π-π stacking, hydrophobic–hydrophilic interactions, and van der Waals forces, are involved in the adsorption process[17].

SEM analysis

SEM images show hydrochar obtained by hydrothermal treatment at three temperatures, i.e. 200 (Fig. 3a), 230 (Fig. 3b), and 260 °C (Fig. 3c), and hydrochar steam-activated at 230 °C (Fig. 3d).

Hydrothermal carbonization leads to a morphological change with the formation of aggregates of microspheres[33]. The SEM image of the hydrochar surface obtained at 200 °C (Fig. 3a) shows the formation of a small number of microspheres. Treatment at 230 °C seems to accelerate the process with the formation of a greater number of aggregates (Fig. 3b), consisting of smaller well-organized spheres of nanometric dimension. These structures decrease in surface area with further increase in temperature from 230 °C to 260 °C, showing a smoother surface and a fibrous structure with few scattered nanospheres (Fig. 3c).

SA-HC-230 shows a noticeable effect on the morphology (Fig. 3d), with an enrichment of aggregates that more homogeneously cover the entire surface. In particular, it is evident that the aggregates consist of compact nanospheres.

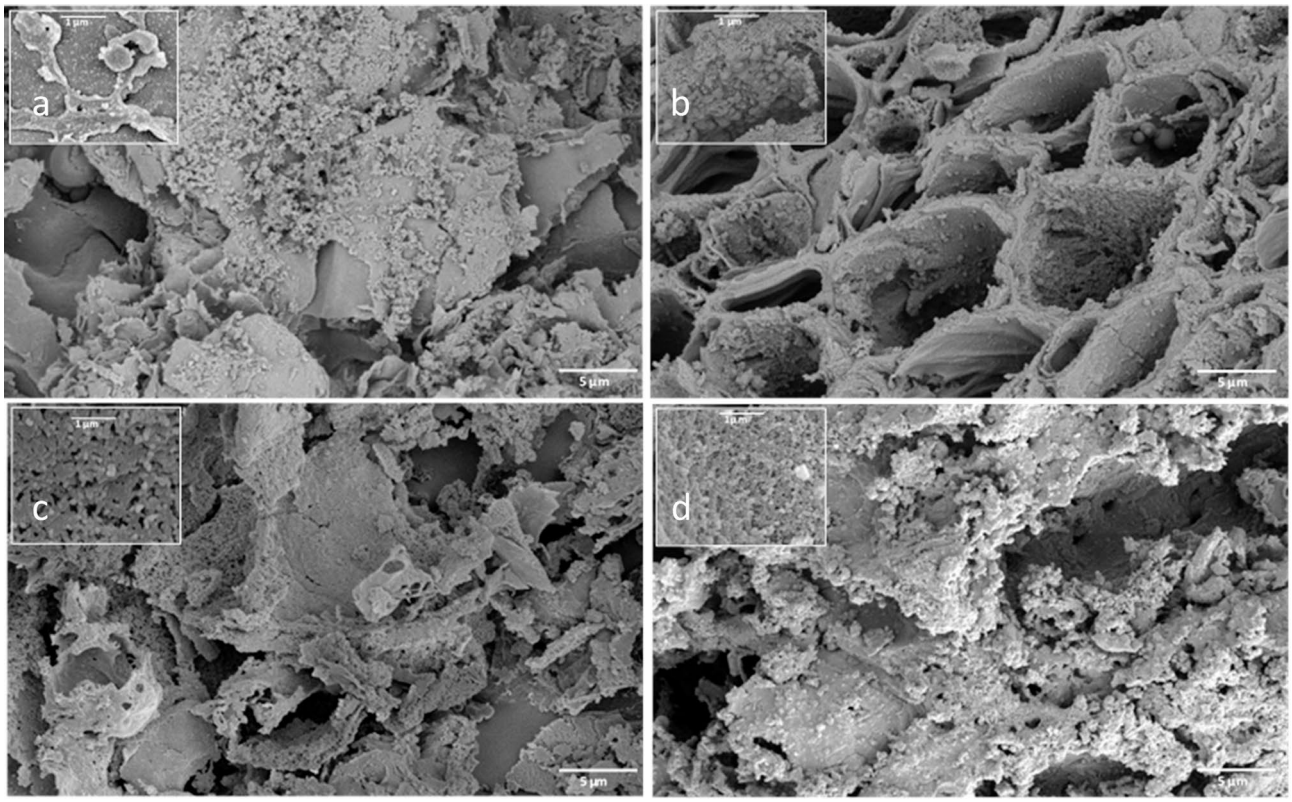

Fig. 3. SEM micrographs (magnification 10,000×) of hydrochar after hydrothermal treatment at 200 (**a**), 230 (**b**), 260 °C (**c**), and steam-activated HC-230 (**d**). Details at 50,000×.

TEM analysis

TEM micrographs of the four different hydrochar samples are shown in Fig. 4. TEM analysis (Fig. 4a) reveals that hydrothermal treatment at 200 °C results in the formation of a loosely structured hydrochar matrix. An increase in the treatment temperature to 230 °C results in a clear change in the morphological composition of the hydrochar, with the appearance of well-structured nanospheres (Fig. 4b). At 260 °C (Fig. 4c), the hydrochar still exhibits a structure with nanospheres, though signs of degradation are evident in certain areas. On the SA-HC-230 (Fig. 4d), the well-organized structure already highlighted in the non-activated sample at 230 °C shows an increase in organization, resulting in a multi-layer flake superstructure composed of nanospheres. The TEM characterization clearly highlights these structural details and aligns with the observations from the SEM morphology.

BET analysis

The key property of adsorbent materials is its adsorption capacity, which is generally proportional to its surface area. Table S2 presents the specific surface area values of the HC-200, HC-230, HC-260, and SA-HC-230 samples. In addition, Fig. 5 displays the N_2 adsorption–desorption isotherms at 77 K of the SA-HC-230 sample. Based on the IUPAC classification, the adsorption characteristics of SA-HC-230 correspond to type IV, as intermediate saturation of the adsorption surface was observed, with a subsequent increase in adsorption at high relative pressures[62].

These results suggest the formation of multilayers during adsorption, indicating that the material can be classified as mesoporous[55]. BET surface area analysis was successfully performed on hydrochar samples produced at 200 °C and 230 °C, yielding values of 17.44 ± 0.20 and 49.41 ± 0.51 m^2 g^{-1}, respectively. Attempts to perform BET analysis on the HC-260 sample were unsuccessful, most likely due to structural collapse or pore blockage induced by over-carbonization at elevated temperature. This hypothesis is consistent with SEM and TEM observations, which revealed a depletion of the porous structure in the HC-260. In comparison, the steam-

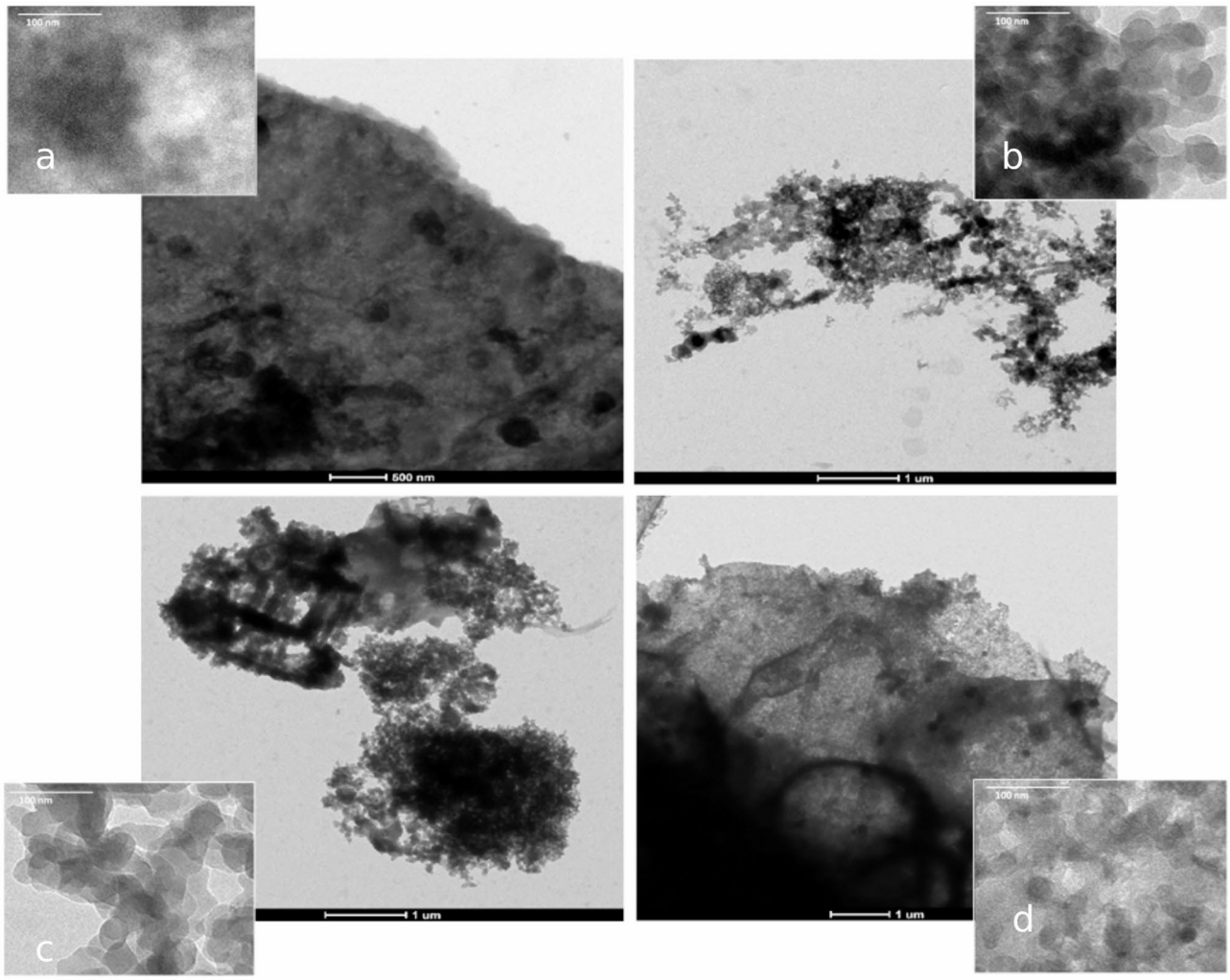

Fig. 4. TEM micrographs (magnification 15,000×) of hydrochar after hydrothermal treatment at 200 (**a**), 230 (**b**), 260 °C (**c**), and steam-activated SA-230 (**d**). Details at 84,000×.

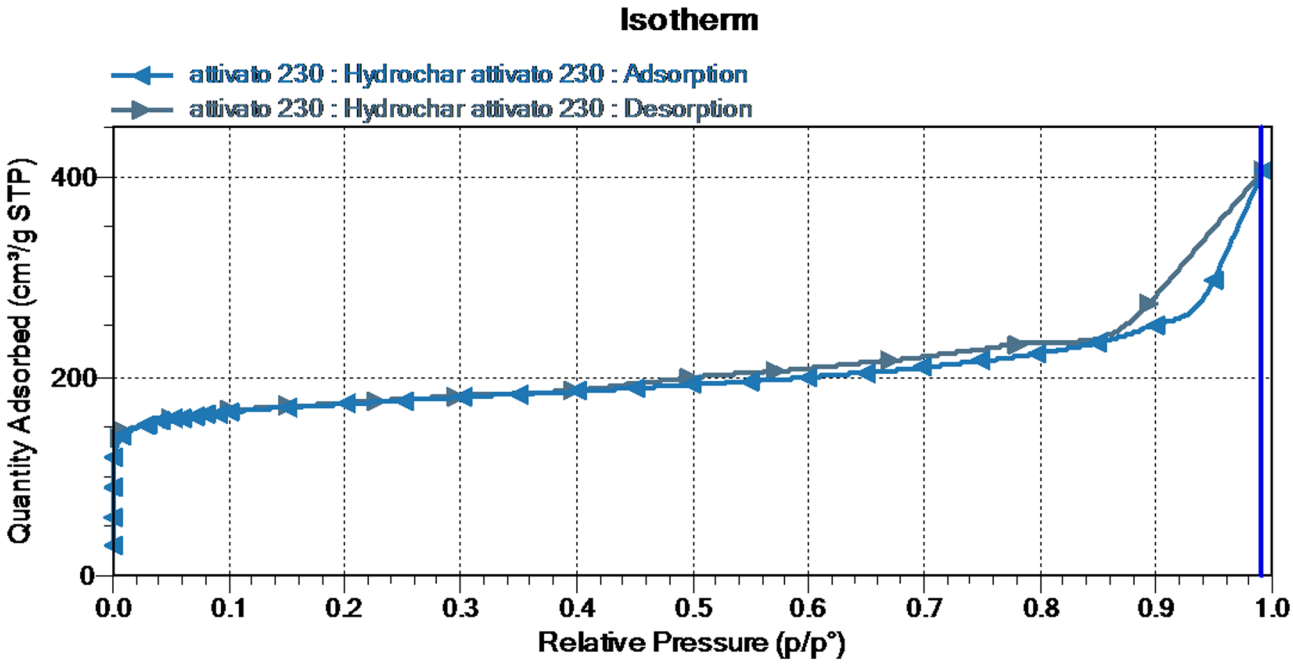

Fig. 5. Adsorption-desorption isotherms of steam-activated HC-230.

HTC temperature (°C)	Adsorbent dosage (g L^{-1})	DCF removal efficiency (%)	Adsorption capacity (mg g^{-1})
200	1.0	11.7	0.67
230	1.0	21.1	1.08
260	1.0	14.7	0.74

Table 3. The effect of HTC operative temperature on hydrochar DCF removal efficiency and adsorption capacity.

activated hydrochar (SA-HC-230) exhibited a markedly higher surface area of 728 ± 5 m^2 g^{-1}. These findings underscore the efficacy of steam activation in significantly enhancing the textural properties of hydrochar.

Diclofenac adsorption

Optimization of HTC temperature

The temperature selected during the HTC process significantly influences the physicochemical characteristics of hydrochar, by facilitating the breakdown of bonds within the biomass's macromolecular structures, consequently impacting the efficiency of DCF removal and the sorbent's adsorption capacity[63]. The impact of the process temperature on the adsorption performance of DCF onto hydrochar is displayed in Fig. S3, and the results are summarized in Table 3. The adsorbent dosage was maintained at 1.0 g L^{-1} across all conditions. Increasing the HTC temperature from 200 to 230 °C led to an enhancement in both DCF removal efficiency % (from 11.7 to 21.1%) and adsorption capacity (from 0.67 to 1.08 mg g^{-1}). Anyway, an additional increase in HTC temperature to 260 °C resulted in a decrease in DCF removal efficiency (14.7%) and adsorption capacity (0.74 mg g^{-1}).

These results can be explained by the SEM and TEM analyses presented earlier, which showed a well-organized nanometric sphere structure in the sample treated at 230 °C. However, for the sample treated at 260 °C, the structure appears to have deteriorated, which may have led to a decrease in surface area. In fact, higher operational temperatures (i.e. 260 °C) can induce more extensive polymerization and carbonization reactions, which in turn reduce the surface area[64]. Similar findings were reported by Soroush et al.[65] when studying the impact of HTC temperature on the physicochemical properties of hydrochar derived from waste seaweed (*Ulva pertusa*). Specifically, as the temperature increased from 180 to 210 °C, the BET surface area of the hydrochar increased from 42.5 to 51.7 m^2 g^{-1}. However, a further increase in temperature to 250 °C resulted in a significant decrease in BET surface area to 37.3 m^2 g^{-1}. Another potential factor may be that, as the reaction continues, organic compounds in the liquid phase undergo polymerization, forming secondary hydrochar. The latter precipitates and masks the primary hydrochar's surface. This process highlights the role of organic compounds dissolved in the liquid phase, which become more influential as reaction temperatures rise[66,67].

DCF adsorption onto activated hydrochar

Although the hydrochar produced at 230 °C showed the highest DCF removal efficiency (%) and adsorption capacity, the material's adsorption performance still lacked. Therefore, HC-230 was steam-activated to enhance contaminant removal during the adsorption process. Figure 6 illustrates the impact of the differences in removal efficiencies (%) and adsorption capacities of HC-230 before and after steam activation, at different adsorbent dosages (0.2–1.0 g L^{-1}).

As depicted in Fig. 6A, the increase in the initial dose of HC-230 led to a slight improvement in DCF removal efficiency (%). The highest value, reaching 21.1%, was attained when 50 mg of HC-230 (adsorbent dosage of 1.0 g L^{-1}) were added into the solution. Increasing the adsorbent dosage is likely to result in a greater number of active sites. Functional groups, which serve as active sites on the adsorbent surface, play a key role in adsorbing contaminants. Therefore, raising the mass of the hydrochar should increase the quantity of functional groups, leading to enhanced adsorption[66]. Nevertheless, as the hydrochar dosage increased, the adsorption capacity decreased from 2.5 to 1.08 mg g^{-1}. The result is probably attributable to phenomena such as aggregation or overlapping of the adsorbent particles, which occur at higher HC-230 dosages, leading to a reduction in the available surface area for DCF adsorption[68]. El-Sayed et al.[69] observed a similar trend carrying out a study on the removal of dyes from impacted water using palm kernel fibers.

Conversely, HC-230 after steam activation exhibited superior adsorption performance. As illustrated in Fig. 6B, increasing the initial adsorbent quantity resulted in a significant enhancement in DCF removal, reaching the highest value of 99.2% at an adsorbent dosage of 1.0 g L^{-1}. This is substantially higher than the removal efficiency achieved using inactivated HC-230 as sorbent. The adsorption capacity decreased from 13.8 to 5.14 mg g^{-1}. This effect could be related to the formation of the multi-layered structure observed in TEM image (Fig. 4d); at high adsorbent dosages, the overlapping of layers could reduce the number of available interaction sites.

Kinetic studies and adsorption isotherms

As mentioned, the kinetic models employed for the DCF adsorption by SA-HC-230 were the pseudo-first order, pseudo-second order, the intra-particle diffusion, and the Elovich model which are commonly used to evaluate different adsorbent materials based on rate constants at various time intervals. The kinetic parameters were determined using the fitting procedure for each experimental run, as illustrated in Fig. S4 and S5, whereas the fitting goodness was tested using the coefficient of determination (R^{234}. As indicated by the data reported in Table 4, the pseudo-second order model fitted better the experimental data for each hydrochar dosage examined. The results are in agreement with previous bibliography for DCF adsorption on hydrochar[34,70].

The initial rate of adsorption h (mg g^{-1} min^{-1}) was given by:

$$h = k_2 {q_e}^2 \tag{14}$$

The increase in the initial DCF adsorption rates (h = 2.42, 2.56, 2.71, and 4.30 mg g^{-1} min^{-1}), with an increase in the adsorbent dosage (from 0.2 to 0.8 g L^{-1}), could be attributed to the increased number of available adsorption sites on the adsorbent. Conversely, the h value of 3.91 mg g^{-1} min^{-1} obtained with a 1.0 g L^{-1} hydrochar dosage confirms the particle aggregation at higher HC-230 dosages and/or secondary hydrochar formation.

Figure 7 presents the experimental data and the fitting process for the Langmuir, Freundlich, Dubinin-Radushkevich, and Temkin adsorption isotherms of DCF on SA-HC-230. The parameters for the adsorption isotherms are detailed in Table S2.

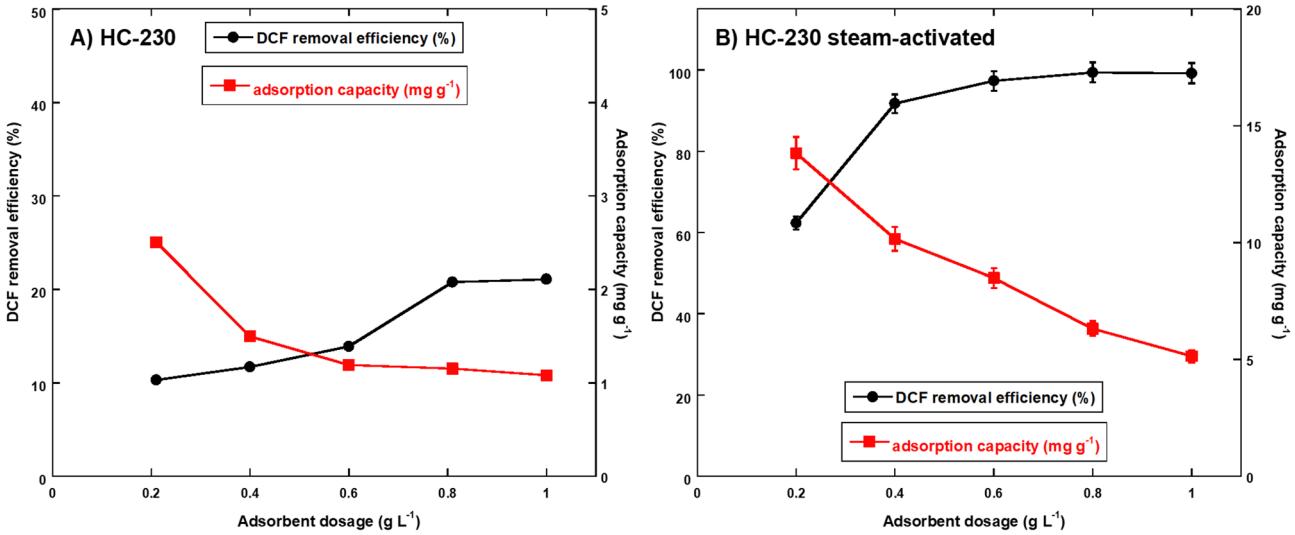

Fig. 6. Effect of adsorbent dosage on DCF removal efficiencies (%) and adsorption capacity of (**A**) HC-230, and (**B**) SA-HC-230; initial DCF concentration = 5.0 mg L^{-1}; pH = 9.0 ± 0.5.

SA-HC-230 (g L^{-1})	0.2	0.4	0.6	0.8	1.0
PFO model					
q_e (mg g^{-1})	16.7	12.2	8.36	6.47	5.15
k_1 (min^{-1})	0.119	0.178	0.247	0.417	0.468
R^2	0.997	0.995	0.997	0.992	0.990
PSO model					
q_e (mg g^{-1})	22.0	14.6	9.50	6.99	5.53
k_2 (mg g^{-1} min^{-1})	0.005	0.012	0.030	0.088	0.128
R^2	0.998	0.999	0.998	0.999	0.999
h (mg g^{-1} min^{-1})	2.42	2.56	2.71	4.30	3.91
IPD model					
K_{id} (mg g^{-1} $min^{-1/2}$)	2.60	1.87	1.47	1.08	0.85
R^2	0.977	0.975	0.935	0.876	0.824
Elovich model					
α (mg g^{-1} min^{-1})	1.54	1.98	3.09	4.97	11.1
β (g mg^{-1})	0.27	0.39	0.53	0.76	1.08
R^2	0.991	0.983	0.970	0.974	0.969

Table 4. Kinetic parameters of the adsorption of DCF on SA-HC-230 at different adsorbent dosage.

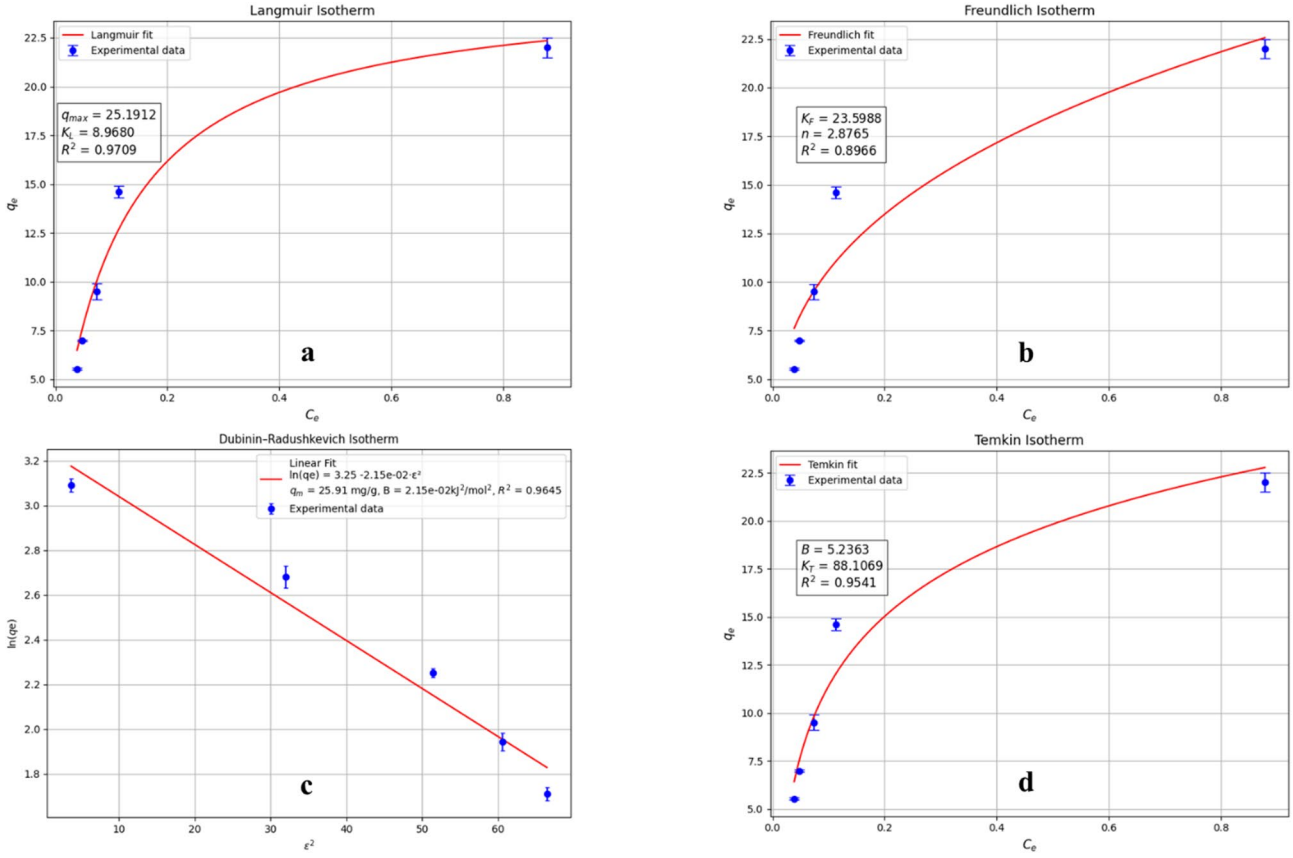

Fig. 7. Isotherm of DCF adsorption on SA-HC-230: (**a**) Langmuir; (**b**) Freundlich; (**c**) Dubinin-Radushkevich; (**d**) Temkin.

The Langmuir model showed a higher correlation coefficient (R^2 = 0.971) compared to the Freundlich (R^2 = 0.897), Dubinin-Radushkevich (R^2 = 0.964), and Temkin (R^2 = 0.954) models. Additionally, the experimental equilibrium capacity (q_e = 22.01 mg g^{-1} was close to the maximum monolayer uptake (q_{max} = 25.19 mg g^{-1} calculated by the Langmuir model. The better fit of the latter isotherm indicates that DCF adsorption on SA-HC-230 may occur predominantly as monolayer coverage on a homogeneous surface with energetically

equivalent sites. This suggests minimal adsorbate-adsorbate interactions and a well-defined saturation capacity. Consequently, the activation process likely enhances surface uniformity, favoring specific adsorption sites[34]. A comparison of the q_{max} of the SA-HC-230 prepared in the current study with values reported in previous works for both physically and chemically activated hydrochars and biomasses is presented in Table 5.

Overall, the SA-HC-230 exhibited a promising adsorption capacity compared to other lignocellulosic-derived adsorbents, particularly those activated by physical methods[70]. Although higher adsorption capacities were achieved in some cases through chemical activation, it should be noted that this method involves higher chemical costs and more complex operational requirements.

Adsorption mechanism analysis

The adsorption behavior of DCF onto SA-HC-230 was examined through analysis of kinetic and equilibrium experimental data. Among the kinetic models tested, the pseudo-second-order model exhibited the highest correlation ($R^2 > 0.998$), implying that chemisorption governs the adsorption rate, likely involving valence interactions through electron sharing or exchange between DCF molecules and the hydrochar's active sites. Regarding equilibrium, the Langmuir isotherm model best represented the data ($R^2 = 0.971$), suggesting monolayer adsorption on a surface with uniform energy distribution. These findings support the involvement of specific interactions, inculding hydrogen bonding, π–π stacking between the aromatic structures of DCF and the hydrochar's graphitic regions, and possible electron exchange with oxygen-containing functional groups, in driving the adsorption mechanism. Although electrostatic repulsion would be expected between the negatively charged surface of the adsorbent (pH_{pzc} = 7.1) and the anionic form of DCF at the operating pH (~ 9.0), high removal efficiencies were nonetheless achieved. This indicates that non-coulombic interactions, such van der Waals forces, and hydrophobic effects, may play a significant role in the adsorption process[17,70]. Additionally, the considerable BET surface area (728 $m^2\ g^{-1}$) and the well-developed mesoporous structure, as revealed by SEM and TEM analyses, suggest that surface diffusion and pore-filling mechanisms could also significantly contribute to DCF uptake[78]. Consequently, the adsorption of DCF onto SA-HC-230 is likely governed by a combination of chemical and physical interactions, where functional surface groups and porosity work synergistically to enhance the overall adsorption capacity.

Reusability studies and practical implication

Evaluating the reusability of the adsorbent is essential for assessing the long-term viability and sustainability of the adsorption process. From an economic perspective, the ability to regenerate and reuse hydrochar over multiple cycles can substantially lower operational costs and reduce the need for fresh material[79]. Moreover, high reusability improves the overall efficiency and practicality of the treatment system, making it more suitable for real-world applications in water purification and the removal of pharmaceutical contaminants. To assess the reusability of SA-HC-230 for DCF adsorption, five successive adsorption–desorption cycles were performed. After each adsorption step, the spent hydrochar was recovered by centrifugation at 6000 rpm for 10 min and thoroughly rinsed with distilled water. Regeneration was performed via thermal treatment[80]. The recovered hydrochar was placed in an oven at 100 °C for 1 h, followed by heating at 200 °C for 3 h. The material was then filtered, repeatedly washed with distilled water until reaching neutral pH, and dried in an oven at 80 °C. The regenerated hydrochar was subsequently reused in a new adsorption test under the same experimental conditions as the initial one. The process was repeated for a total of five cycles.

The results shown in Fig. 8 revealed that SA-HC-230 preserved an high DCF removal efficiency over multiple consecutive cycles. Specifically, after the fifth cycle, the DCF removal efficiency remained as high as 95%, confirming the excellent reusability and long-term adsorption performance of SA-HC-230, and highlighting its potential for practical applications. These results are in line with previous studies[70,81]. This not only contributes to a reduction in operating costs but also decreases the need for fresh adsorbent material. Furthermore, the use of grape stalks, an abundant and low-cost agricultural by-product, as the raw material for SA-HC-230 production makes the overall process economically and environmentally advantageous. Despite these promising outcomes, it is important to acknowledge that further long-term studies under continuous-flow conditions and with real wastewater are necessary to fully validate the material's stability and practical applicability, offering a valuable direction for future research.

Biomass	Activation method	S_{BET} ($m^2\ g^{-1}$)	q_{max} (mg g^{-1})	Ref.
Orange peel	Physical by air	499	5.73	[71]
Cocoa pod husks	Chemical by H_2SO_4	/	5.53	[72]
Potato peel	Chemical by K_2CO_3	866	68.5	[73]
Olive-waste cake	Chemical by H_3PO_4	/	56.2	[74]
Palm kernel shells	Physical by nitrogen flow	131	13.16	[70]
Moringa seed powder	Chemical activation by H_3PO_4	/	100.9	[75]
Rice hull	Torrefied at 350 °C	/	3.30	[76]
Orange peel	Physical by CO_2	301	1.91	[71]
Cyclamen persicum tubers	Chemical activation by $ZnCl_2$	881	22.2	[77]
Grape stalk	Physical by steam	731	25.19	This study

Table 5. Comparison of the maximum DCF adsorption capacities of various biomass-derived adsorbents.

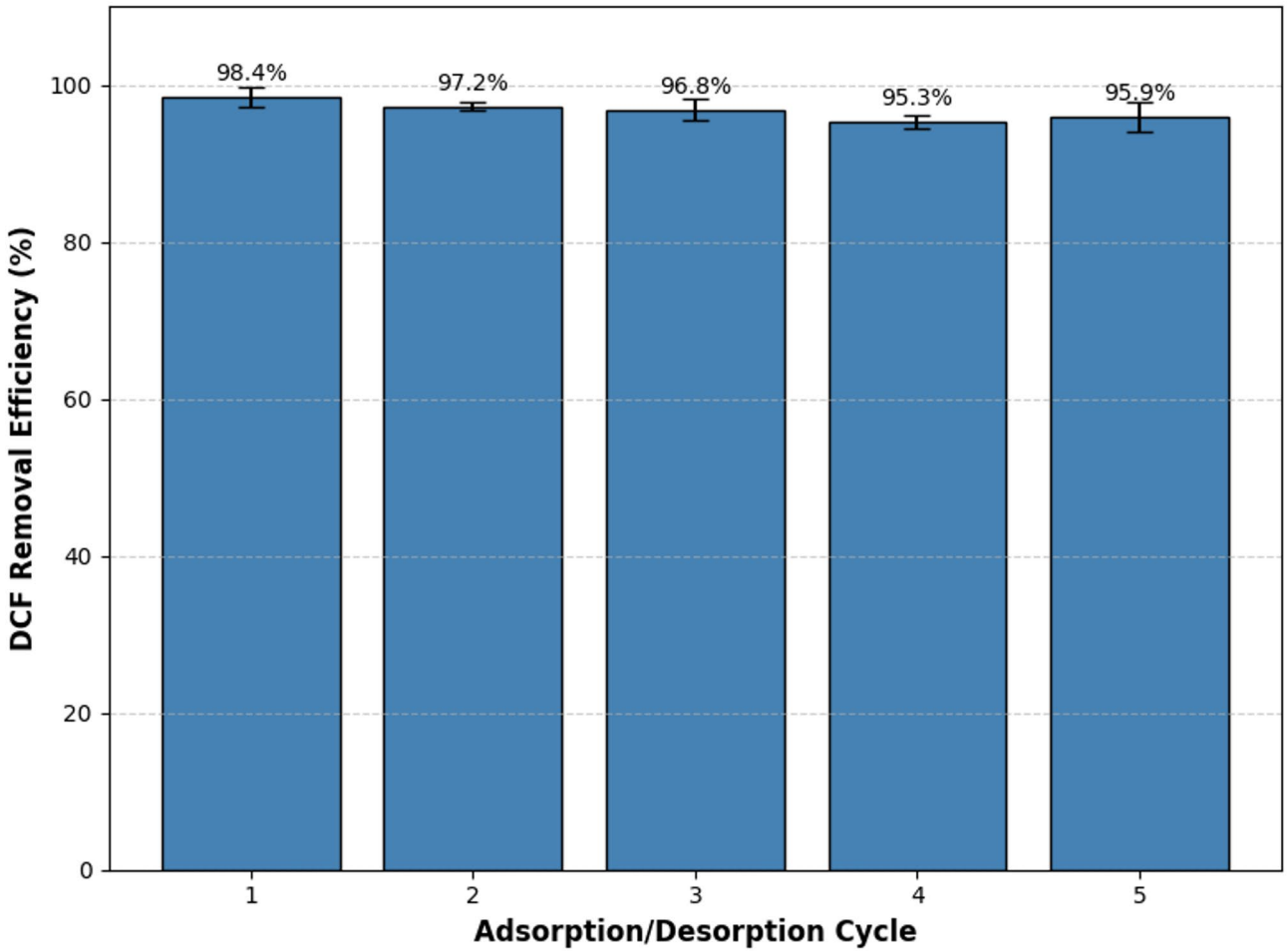

Fig. 8. Evaluation of SA-HC-230 reusability through five successive adsorption–desorption cycles.

Conclusions

This work highlights the successful transformation of grape stalks, an abundant agricultural by-product, into an effective adsorbent for diclofenac removal from water using hydrothermal carbonization and subsequent steam activation. Among the tested hydrothermal carbonization process conditions, 230 °C was identified as the optimal temperature for producing hydrochar with enhanced adsorption properties. The subsequent steam activation further improved the hydrochar effectiveness by increasing its surface area and porosity. The activated hydrochar demonstrated a maximum diclofenac removal efficiency of 99.2% and an adsorption capacity of 25.19 mg g^{-1}. The adsorption process was most accurately represented by the pseudo-second-order kinetic model and the Langmuir isotherm, indicating a chemisorption mechanism occurring on a homogeneous surface. Nonetheless, other interaction pathways, such as hydrogen bonding, π–π interactions, and intraparticle diffusion, also seem to contribute. These findings suggest that the overall adsorption is driven by a synergistic combination of chemical and physical forces. In addition, the results indicate that the steam-activated hydrochar maintains high diclofenac removal efficiency over multiple cycles (>95%) after the fifth cycle, demonstrating its excellent reusability and long-term adsorption performance. This implies a reduction in operating costs and minimization of the required amount of fresh adsorbent. Nonetheless, additional long-term studies with real wastewater are needed to fully validate the stability and practical applicability of the steam-activated hydrochar.

Despite the encouraging performance of the steam-activated hydrochar derived from waste grape stalks in the removal of diclofenac, several limitations still need to be addressed for its practical implementation. The primary environmental concern stems from the liquid by-product produced during the hydrothermal carbonization process, which is rich in dissolved organic compounds such as carboxylic acids, phenols, and furfural[82]. Key issues include recovering these valuable compounds from process water, optimizing the use of the additional water required for the process, and properly disposing of residual liquid by-products. The application of advanced oxidation processes, such as electrochemical oxidation, offers a promizing strategy for treating the liquid effluent generated during the hydrothermal carbonization process. This approach could effectively remove organic contaminants, facilitating internal water reuse within a closed-loop system[83]. These advancements will help unlock the long-term environmental potential of this sustainable adsorbent.

Data availability

The data that support the findings of this study are available from the corresponding author, upon reasonable request.

Received: 16 April 2025; Accepted: 6 August 2025
Published online: 01 October 2025

References

1. Feng, J. B., Li, Y., Zhang, Y., Xu, Y. & Cheng, X. W. Adsorptive removal of indomethacin and diclofenac from water by polypyrrole doped-GO/COF-300 nanocomposites. *Chem. Eng. J.* **429**, 132499 (2022).
2. Salomão, G. R. et al. Diclofenac removal in water supply by adsorption on composite low-cost material. *Environ. Technol.* **42**, 2095–2111 (2021).
3. Bhadra, B. N., Seo, P. W. & Jhung, S. H. Adsorption of diclofenac sodium from water using oxidized activated carbon. *Chem. Eng. J.* **301**, 27–34 (2016).
4. Dzimitrowicz, A. et al. Biosafe removal of diclofenac from wastewaters by a continuous-flow mode cold atmospheric pressure plasma system. *J. Environ. Chem. Eng.* **12**, 111598 (2024).
5. Larous, S. & Meniai, A. H. Adsorption of diclofenac from aqueous solution using activated carbon prepared from Olive stones. *Int. J. Hydrogen Energy*. **41**, 10380–10390 (2016).
6. De Oliveira, T. et al. Adsorption of diclofenac onto organoclays: effects of surfactant and environmental (pH and temperature) conditions. *J. Hazard. Mater.* **323**, 558–566 (2017).
7. aus der Beek, T. et al. Pharmaceuticals in the environment—Global occurrences and perspectives. *Environ. Toxicol. Chem.* **35**, 823–835 (2015).
8. Cavalheri, P. S. et al. Ketoprofen and diclofenac removal and toxicity abatement in a real scale sewage treatment plant by photo-Fenton process with design of experiments. *J. Environ. Chem. Eng.* **11**, 110699 (2023).
9. Sousa, J. C. G., Ribeiro, A. R., Barbosa, M. O., Pereira, M. F. R. & Silva, A. M. T. A review on environmental monitoring of water organic pollutants identified by EU guidelines. *J. Hazard. Mater.* **344**, 146–162 (2018).
10. Rigueto, C. V. T. et al. Adsorption of diclofenac sodium by composite beads prepared from tannery wastes-derived gelatin and carbon nanotubes. *J. Environ. Chem. Eng.* **9**, 105030 (2021).
11. Farah, M. et al. Intensification of diclofenac removal through supported liquid membrane and ozonation. *Environ. Technol. Innov.* **33**, 103469 (2024).
12. Alessandretti, I., Rigueto, C. V. T., Nazari, M. T., Rosseto, M. & Dettmer, A. Removal of diclofenac from wastewater: A comprehensive review of detection, characteristics and tertiary treatment techniques. *J. Environ. Chem. Eng.* **9**, 106743 (2021).
13. Conte, F. et al. Comparison of Different Advanced Oxidation Processes (AOPs) and Photocatalysts for the Degradation of Diclofenac. *ChemPhotoChem* 8, (2024).
14. Iovino, P. et al. An integrated approach for the assessment of the electrochemical oxidation of diclofenac: By-product identification, Microbiological and eco-genotoxicological evaluation. *Sci. Total Environ.* **909**, 168511 (2024).
15. Licona, K. P. M. et al. Assessing potential of nanofiltration and reverse osmosis for removal of toxic pharmaceuticals from water. *J. Water Process. Eng.* **25**, 195–204 (2018).
16. Danso-Boateng, E. et al. Production and characterisation of adsorbents synthesised by hydrothermal carbonisation of biomass wastes. *SN Appl. Sci.* **3**, 257 (2021).
17. Salvestrini, S., Fenti, A., Chianese, S., Iovino, P. & Musmarra, D. Diclofenac sorption from synthetic water: kinetic and thermodynamic analysis. *J. Environ. Chem. Eng.* **8**, 104105 (2020).
18. Chu, Y. et al. The enhanced adsorption of diclofenac sodium (DCF) and ibuprofen (IBU) on modified montmorillonite with benzyldimethylhexadecylammonium chloride (HDBAC). *Colloids Surf. Physicochem Eng. Asp.* **681**, 132764 (2024).
19. Chianese, S., Fenti, A., Blotevogel, J., Musmarra, D. & Iovino, P. Trimethoprim removal from wastewater: adsorption and electro-oxidation comparative case study. *Case Stud. Chem. Environ. Eng.* **8**, 100433 (2023).
20. Pereira, A. G. B., Rodrigues, F. H. A., Paulino, A. T., Martins, A. F. & Fajardo, A. R. Recent advances on composite hydrogels designed for the remediation of dye-contaminated water and wastewater: A review. *J. Clean. Prod.* **284**, 124703 (2021).
21. Lv, B. W., Xu, H., Guo, J. Z., Bai, L. Q. & Li, B. Efficient adsorption of methylene blue on carboxylate-rich hydrochar prepared by one-step hydrothermal carbonization of bamboo and acrylic acid with ammonium persulphate. *J. Hazard. Mater.* **421**, 126741 (2022).
22. Donar, Y. O., Çağlar, E. & Sınağ, A. Preparation and characterization of agricultural waste biomass based hydrochars. *Fuel* **183**, 366–372 (2016).
23. Hassan, M. M. & Carr, C. M. Biomass-derived porous carbonaceous materials and their composites as adsorbents for cationic and anionic dyes: A review. *Chemosphere* **265**, 129087 (2021).
24. Chew, K. W. et al. Abatement of hazardous materials and biomass waste via pyrolysis and co-pyrolysis for environmental sustainability and circular economy. *Environ. Pollut.* **278**, 116836 (2021).
25. Filippov, S. P. & Keiko, A. V. Coal gasification: at the crossroad. Technological factors. *Therm. Eng.* **68**, 209–220 (2021).
26. Piersa, P. et al. An extensive review and comparison of modern biomass torrefaction reactors vs. biomass Pyrolysis—Part 1. *Energies* **15**, 2227 (2022).
27. Zaccariello, L. & Montagnaro, F. Fluidised bed gasification of biomasses and wastes to produce hydrogen-rich syn-gas – a review. *J. Chem. Technol. Biotechnol.* **98**, 1878–1887 (2023).
28. Mastellone, M. L. & Zaccariello, L. Gasification of polyethylene in a bubbling fluidized bed operated with the air staging. *Fuel* **106**, 226–233 (2013).
29. Wang, T., Zhai, Y., Zhu, Y., Li, C. & Zeng, G. A review of the hydrothermal carbonization of biomass waste for hydrochar formation: process conditions, fundamentals, and physicochemical properties. *Renew. Sustain. Energy Rev.* **90**, 223–247 (2018).
30. Supee, A. H. & Zaini, M. A. A. Hydrothermal carbonization of biomass: a commentary. *Fullerenes Nanotub Carbon Nanostruct.* **32**, 119–127 (2024).
31. Masoumi, S., Borugadda, V. B., Nanda, S., Dalai, A. K. & Hydrochar A review on its production technologies and applications. *Catalysts* **11**, 939 (2021).
32. Battipaglia, G. et al. Hydrochar application improves growth and intrinsic water use efficiency of Populus alba, especially during hot season. *Forests* **14**, 658 (2023).
33. Zhang, Y., Jiang, Q., Xie, W., Wang, Y. & Kang, J. Effects of temperature, time and acidity of hydrothermal carbonization on the hydrochar properties and nitrogen recovery from corn Stover. *Biomass Bioenerg.* **122**, 175–182 (2019).
34. Oumabady, S. et al. Kinetic and isotherm insights of diclofenac removal by sludge derived hydrochar. *Sci. Rep.* **12**, 2184 (2022).
35. Sulaiman, N. S., Hashim, R., Mohamad Amini, M. H., Danish, M. & Sulaiman, O. Optimization of activated carbon Preparation from cassava stem using response surface methodology on surface area and yield. *J. Clean. Prod.* **198**, 1422–1430 (2018).
36. Rashid, R. A., Jawad, A. H., Ishak, M. A. M. & Kasim, N. N. KOH-activated carbon developed from biomass waste: adsorption equilibrium, kinetic and thermodynamic studies for methylene blue uptake. *Desalin. Water Treat.* **57**, 27226–27236 (2016).

37. Zaccariello, L., Mastellone, M. L., D'Amelia, L. I., Catauro, M. & Morrone, B. Assessment of integration between lactic acid, biogas and hydrochar production in OFMSW plants. *Energies* **13**, 6593 (2020).
38. Wang, T. et al. Influence of temperature on nitrogen fate during hydrothermal carbonization of food waste. *Bioresour Technol.* **247**, 182–189 (2018).
39. Zaccariello, L., Battaglia, D., Morrone, B. & Mastellone, M. L. Hydrothermal carbonization: A Pilot-Scale reactor design for Bio-waste and sludge Pre-treatment. *Waste Biomass Valoriz.* **13**, 3865–3876 (2022).
40. Aragón-Briceño, C. I. et al. Hydrothermal carbonization of wet biomass from nitrogen and phosphorus approach: A review. *Renew. Energy*. **171**, 401–415 (2021).
41. Ischia, G. & Fiori, L. Hydrothermal carbonization of organic waste and biomass: A review on process, reactor, and plant modeling. *Waste Biomass Valoriz.* **12**, 2797–2824 (2021).
42. Khan, N., Mohan, S. & Dinesha, P. Regimes of hydrochar yield from hydrothermal degradation of various lignocellulosic biomass: A review. *J. Clean. Prod.* **288**, 125629 (2021).
43. Azzaz, A. A., Khiari, B., Jellali, S., Ghimbeu, C. M. & Jeguirim, M. Hydrochars production, characterization and application for wastewater treatment: A review. *Renew. Sustain. Energy Rev.* **127**, 109882 (2020).
44. González, J. F., Román, S., González-García, C. M., Nabais, J. M. V. & Ortiz, A. L. Porosity development in activated carbons prepared from walnut shells by carbon dioxide or steam activation. *Ind. Eng. Chem. Res.* **48**, 7474–7481 (2009).
45. Channiwala, S. A. & Parikh, P. P. A unified correlation for estimating HHV of solid, liquid and gaseous fuels. *Fuel* **81**, 1051–1063 (2002).
46. Zaccariello, L. & Mastellone, M. L. Fuel gas production from the Co-Gasification of coal, plastic waste, and wood in a fluidized bed reactor: effect of gasifying agent and bed material. *Sustainability* **15**, 7547 (2023).
47. Montagnaro, F. & Zaccariello, L. Performance assessment of a demonstration-scale biomass gasification power plant using material and energy flow analyses. *Energy* **284**, 129327 (2023).
48. Chatir, E. M., Hadrami, E. L., Ojala, A., Brahmi, R. & S. & Thermal treatment of H3PO4-impregnated hydrochar under controlled oxygen flows for producing materials with tunable properties and enhanced diclofenac adsorption. *Sustain. Chem. Pharm.* **34**, 101164 (2023).
49. Phan, K. A., Phihusut, D. & Tuntiwiwattanapun, N. Preparation of rice husk hydrochar as an atrazine adsorbent: optimization, characterization, and adsorption mechanisms. *J. Environ. Chem. Eng.* **10**, 107575 (2022).
50. Jung, K. W., Lee, S. Y., Choi, J. W., Hwang, M. J. & Shim, W. G. Synthesis of Mg–Al layered double hydroxides-functionalized hydrochar composite via an in situ one-pot hydrothermal method for arsenate and phosphate removal: structural characterization and adsorption performance. *Chem. Eng. J.* **420**, 129775 (2021).
51. Fenti, A. & Salvestrini, S. Analytical solution of the Langmuir-based linear driving force model and its application to the adsorption kinetics of boscalid onto granular activated carbon. *React. Kinet Mech. Catal.* **125**, 1–13 (2018).
52. Chianese, S., Fenti, A., Iovino, P., Musmarra, D. & Salvestrini, S. Sorption of organic pollutants by humic acids: A review. *Molecules* **25**, 918 (2020).
53. Vareda, J. P. On validity, physical meaning, mechanism insights and regression of adsorption kinetic models. *J. Mol. Liq.* **376**, 121416 (2023).
54. Hayoun, B. et al. Preparation and characterization of high performance hydrochar for efficient adsorption of drugs mixture. *J. Mol. Liq.* **353**, 118797 (2022).
55. Congsomjit, D. & Areeprasert, C. Hydrochar-derived activated carbon from sugar cane Bagasse employing hydrothermal carbonization and steam activation for syrup decolorization. *Biomass Convers. Biorefinery.* **11**, 2569–2584 (2021).
56. Teğin, İ., Demirel, M. F., Alacabey, İ. & Yabalak, E. Investigation of the effectiveness of waste nut shell–based hydrochars in water treatment: a model study for the adsorption of methylene blue. *Biomass Convers. Biorefinery*. **14**, 10399–10412 (2024).
57. Azizian, S., Eris, S. & Wilson, L. D. Re-evaluation of the century-old Langmuir isotherm for modeling adsorption phenomena in solution. *Chem. Phys.* **513**, 99–104 (2018).
58. Szostak, K., Hodacka, G., Długosz, O., Pulit-Prociak, J. & Banach, M. Sorption of mercury in batch and Fixed-Bed column system on hydrochar obtained from Apple pomace. *Processes* **10**, 2114 (2022).
59. Gole, P., Raut, K. & Kandasubramanian, B. Polymer-based Biochar materials for environmental remediation: A review. *Hybrid. Adv.* **6**, 100267 (2024).
60. Chauhan, S., Shafi, T., Dubey, B. K. & Chowdhury, S. Biochar-mediated removal of pharmaceutical compounds from aqueous matrices via adsorption. *Waste Dispos. Sustain. Energy*. **5**, 37–62 (2023).
61. Yu, S. et al. From biomass to hydrochar: evolution on elemental composition, morphology, and chemical structure. *J. Energy Inst.* **101**, 194–200 (2022).
62. Ng, K. C., Burhan, M., Shahzad, M. W. & Ismail, A. Bin. A universal isotherm model to capture adsorption uptake and energy distribution of porous heterogeneous surface. *Sci. Rep.* **7**, 10634 (2017).
63. Stemann, J., Putschew, A. & Ziegler, F. Hydrothermal carbonization: process water characterization and effects of water recirculation. *Bioresour Technol.* **143**, 139–146 (2013).
64. Bai, K., Hao, J., Yang, Y. & Qian, A. The effect of hydrothermal temperature on the properties of SBA-15 materials. *Heliyon* **6**, e04436 (2020).
65. Soroush, S. et al. Production of solid hydrochar from waste seaweed by hydrothermal carbonization: effect of process variables. *Biomass Convers. Biorefinery*. **14**, 183–197 (2024).
66. Volpe, M. & Fiori, L. From Olive waste to solid biofuel through hydrothermal carbonisation: the role of temperature and solid load on secondary Char formation and hydrochar energy properties. *J. Anal. Appl. Pyrol.* **124**, 63–72 (2017).
67. Zheng, M., Li, X. & Guo, L. Dynamic trends for char/soot formation during secondary reactions of coal pyrolysis by large-scale reactive molecular dynamics. *J. Anal. Appl. Pyrol.* **155**, 105048 (2021).
68. Etim, U. J., Umoren, S. A. & Eduok, U. M. Coconut Coir dust as a low cost adsorbent for the removal of cationic dye from aqueous solution. *J. Saudi Chem. Soc.* **20**, S67–S76 (2016).
69. El-Sayed, G. O. Removal of methylene blue and crystal Violet from aqueous solutions by palm kernel fiber. *Desalination* **272**, 225–232 (2011).
70. Kimbi Yaah, V. B., Zbair, M., Botelho de Oliveira, S. & Ojala, S. Hydrochar-derived adsorbent for the removal of diclofenac from aqueous solution. *Nanotechnol Environ. Eng.* **6**, 3 (2021).
71. Fernandez, M. E., Ledesma, B., Román, S., Bonelli, P. R. & Cukierman, A. L. Development and characterization of activated hydrochars from orange peels as potential adsorbents for emerging organic contaminants. *Bioresour Technol.* **183**, 221–228 (2015).
72. de Luna, M. D. G., Murniati, Budianta, W., Rivera, K. K. P. & Arazo, R. O. Removal of sodium diclofenac from aqueous solution by adsorbents derived from cocoa pod husks. *J. Environ. Chem. Eng.* **5**, 1465–1474 (2017).
73. Bernardo, M. et al. High efficacy on diclofenac removal by activated carbon produced from potato Peel waste. *Int. J. Environ. Sci. Technol.* **13**, 1989–2000 (2016).
74. Baccar, R., Sarrà, M., Bouzid, J., Feki, M. & Blánquez, P. Removal of pharmaceutical compounds by activated carbon prepared from agricultural by-product. *Chem. Eng. J.* **211–212**, 310–317 (2012).
75. Bagheri, A., Abu-Danso, E., Iqbal, J. & Bhatnagar, A. Modified Biochar from Moringa seed powder for the removal of diclofenac from aqueous solution. *Environ. Sci. Pollut Res.* **27**, 7318–7327 (2020).
76. Filipinas, J. Q. et al. Removal of sodium diclofenac from aqueous solutions by rice hull Biochar. *Biochar* **3**, 189–200 (2021).

77. Jodeh, S., Abdelwahab, F., Jaradat, N., Warad, I. & Jodeh, W. Adsorption of diclofenac from aqueous solution using *Cyclamen persicum* tubers based activated carbon (CTAC). *J. Assoc. Arab. Univ. Basic. Appl. Sci.* **20**, 32–38 (2016).
78. Zhong, H. et al. Efficient adsorption removal of carbamazepine from water by dual-activator modified hydrochar. *Sep. Purif. Technol.* **353**, 128287 (2025).
79. Khanzada, A. K. et al. Hydrochar as a bio-based adsorbent for heavy metals removal: A review of production processes, adsorption mechanisms, kinetic models, regeneration and reusability. *Sci. Total Environ.* **945**, 173972 (2024).
80. Cuccarese, M. et al. Removal of diclofenac from aqueous solutions by adsorption on thermo-plasma expanded graphite. *Sci. Rep.* **11**, 3427 (2021).
81. Sachan, D. & Das, G. Selective adsorption of drug micropollutants from synthetic wastewater using hydrochar derived from carbonisation of unused leaves. *Int. J. Environ. Anal. Chem.* **104**, 7–26 (2024).
82. Liakos, D., Altiparmaki, G., Moustakas, K., Malamis, S. & Vakalis, S. The fate of volatile fatty acids (VFAs) during the thermodynamic transition from hydrothermal carbonization to hydrothermal liquefaction: HtC-to-HtL. *Sustain. Chem. Pharm.* **41**, 101683 (2024).
83. Wang, R. et al. Design and operational performance evaluation of an integrated hydrothermal carbonization waste heat recovery and solar energy collection system. *Energy* **321**, 135472 (2025).

Author contributions

L.Z., A.T., A.F., G.F., S.G., D.P., A.G., M.T. conducted experiments and carried out formal data analysis. L.Z., A.F., P.I., M.T. contributed to the design of the study. L.Z., P.I., M.T provided resources and supervised the research. All Authors contributed to the writing and reviewed the manuscript.

Declarations

Competing interests

The authors declare no competing interests.

Ethics declarations

This study did not involve any human samples and was approved by all authors.

Additional information

Supplementary Information The online version contains supplementary material available at https://doi.org/10.1038/s41598-025-15211-5.

Correspondence and requests for materials should be addressed to A.F.

Reprints and permissions information is available at www.nature.com/reprints.

Publisher's note Springer Nature remains neutral with regard to jurisdictional claims in published maps and institutional affiliations.